https://doi.org/10.5194/acp-2021-890
Preprint. Discussion started: 8 November 2021

Atmospheric Chemistry and Physics Discussions

OH-Initiated Atmospheric Degradation of Hydroxyalkyl Hydroperoxides: Mechanism, Kinetics, and Structure-Activity Relationship

Long Chen,[1,2] Yu Huang, *[,1,2] Yonggang Xue, [1,2] Zhihui Jia,[3] Wenliang Wang[4]

[1] *State Key Lab of Loess and Quaternary Geology (SKLLQG), Institute of Earth Environment, Chinese Academy of Sciences (CAS), Xi'an, 710061, China*

[2] *CAS Center for Excellence in Quaternary Science and Global Change, Xi'an, 710061, China*

[3] *School of Materials Science and Engineering, Shaanxi Normal University, Xi'an, Shaanxi, 710119, China*

[4] *School of Chemistry and Chemical Engineering, Key Laboratory for Macromolecular Science of Shaanxi Province, Shaanxi Normal University, Xi'an, Shaanxi, 710119, China*

*Corresponding author:

Prof. Yu Huang, E-mail address: huangyu@ieecas.cn

https://doi.org/10.5194/acp-2021-890
Preprint. Discussion started: 8 November 2021

Atmospheric Chemistry and Physics Discussions

Abstract:

Hydroxyalkyl hydroperoxides (HHPs), formed in the reactions of Criegee intermediates (CIs) with water vapour, play essential roles in the formation of secondary organic aerosol (SOA) under atmospheric conditions. However, the transformation mechanism for OH-initiated oxidation of HHPs is remain incompletely understood. Herein, the quantum chemical and kinetics modeling methods are applied to insight into the detailed mechanisms of OH-initiated oxidation of distinct HHPs formed form the reactions of CH_2OO, *anti*-CH_3CHOO and $(CH_3)_2COO$) with water vapor. The calculations show that H-abstraction by OH radical from the -OOH group of distinct HHPs is predominate as the main products peroxyl radicals (RO_2), and the barrier of dominant pathway is increased as the number of methyl group is increased. In pristine environments, the self-reaction of RO_2 radical initially produces tetroxide intermediate via a head-to-head interaction, then it decomposes into propagation and termination products through the asymmetric two-step O-O bond scission, in which the rate-limiting step is the first O-O bond cleavage. The barrier height of distinct RO_2 radicals reactions with HO_2 radical is independent on the number of methyl substitution. Compared to the rate coefficient of parent system, it is increased by a factor of 3-5 when one or two methyl groups introduce into the C1-position. The autoxidation of RO_2 radicals are unlikely to proceed in the atmosphere due to their dramatically high barriers and strongly endergonic. In urban environments, the rate-limiting step is the hydrogen abstraction by O_2 in the processes of $HOCH_2OO$ radical reaction with NO, while it becomes the O-O bond scission when one or two methyl substitutions occur at the C1-position of $HOCH_2OO$ radical. These new findings are expected to deepen our current understanding for the photochemistry oxidation of hydroperoxides under realistic atmospheric conditions.

https://doi.org/10.5194/acp-2021-890
Preprint. Discussion started: 8 November 2021

Atmospheric Chemistry and Physics Discussions

1. Introduction

Hydroxyalkyl hydroperoxides (HHPs), generated via the reactions of Criegee intermediates (CIs) with water vapour, play important roles in the formation of secondary organic aerosol (SOA) (Qiu et al., 2019; Kumar et al., 2014). The CIs formed from the ozonolysis of alkenes are characterized by high reactivity and excess energies, which can proceed either prompt unimolecular decay to OH radical or, after collisional stabilization, bimolecular reactions with various trance gases like SO_2, NO_2 and H_2O to produce sulfate, nitrate and SOA, thereby influencing air quality and human health (Lester and Klippenstein, 2018; Chen et al., 2017, 2019; Liu et al., 2019; Chhantyal-Pun et al., 2017; Anglada and Solé, 2016; Gong and Chen, 2021). Among these reactions, the bimolecular reaction of CIs with water is thought to be the dominant chemical sink because its concentration (1.3-8.3 $\times 10^{17}$ molecules cm^{-3}) is several orders of magnitude greater than those of SO_2 and NO_2 (~ 10^{12} molecules cm^{-3}) in the atmosphere (Huang et al., 2015; Khan et al., 2018; Taatjes et al., 2013, 2017). The primary products of CIs reactivity toward water are highly oxygenated HHPs that are difficult to detect and identify by using the available analytical techniques due to their thermally instability (Qiu et al., 2019; Anglada et al., 2016; Chao et al., 2015; Chen et al., 2016a; Ryzhkov and Ariya, 2003).

HHPs, due to the presence of both hydroxyl and perhydroxy moieties, have relatively low volatility and vapor pressure contributing substantially to the formation and growth of SOA (Qiu et al., 2019). The atmospheric degradation of HHPs initiated by OH radical is expected to be one of the dominant loss processes because OH radical is the most powerful oxidizing agent (Gligorovski et al., 2015; Allen et al., 2018). Reaction with OH radical includes three possible H-abstraction channels: (a) the alkyl hydrogen, (b) the -OH hydrogen, and (c) the -OOH hydrogen, which is followed by further reactions to generate organic peroxyl radicals (RO_2) as reactive intermediates (Allen et al., 2018). Based on our current mechanistic understanding, RO_2 radicals have three possible channels in pristine environments: (1) they can proceed self- and cross-reactions resulting in formation of alkoxy radical RO, alcohol,

https://doi.org/10.5194/acp-2021-890
Preprint. Discussion started: 8 November 2021


Atmospheric Chemistry and Physics Discussions

carbonyl, accretion products (Berndt et al., 2018; Zhang et al., 2012; Valiev et al., 2019); (2) they can react with HO_2 radical leading to the formation of closed-shell hydroperoxide (ROOH), RO ; OH radical, etc.; (Dillon and Crowley, 2008; Iyer et al., 2018) (3) they can undergo autoxidation via intramolecular H-shift and alternating O_2-addition steps producing highly oxygenated organic molecules (HOMs), which have been identified as the low vapour pressure and low volatility compounds that contribute to the formation and growth of SOA (Crounse et al., 2013; Jokinen et al., 2014; Wang et al., 2018; Ehn et al., 2014; Iyer et al., 2021). In urban environments, RO_2 radicals can react with NO_x generating peroxynitrate (RO_2NO_2), organic nitrate ($RONO_2$), RO ·and other SOA precursors (Wang et al., 2017; Xu et al., 2014, 2020; Ma et al., 2021). The relative importance of distinct pathways depends strongly on the nature of RO_2 radicals and the concentrations of coreactants.

Hydroxymethyl hydroperoxide (HMHP, $HOCH_2OOH$), the simplest HHPs from the reaction of CH_2OO with water, has received considerable scientific attention in recent years because of its high mixing ratios under conditions of forested regions (~ 5 ppbv) (Kumar et al., 2014; Allen et al., 2018; Francisco and Eisfeld, 2009). A recent experimental study by Allen et al. (2018) conducted the OH-initiated oxidation of HMHP in an environmental chamber and simulated the impact of HMHP oxidation on the global formic acid concentrations using the chemical transport model GEOS-Chem. It was found that H-abstraction from the methyl group of HMHP results in formic acid, and it contributes to the global formic acid production about 1.7 Tg yr^{-1}. Francisco and Eisfeld (2009) by employing *ab initio* CCSD(T)//MP2 methods, studied the atmospheric oxidation mechanism of HMHP initiated by OH radical, arriving at the same conclusion that the degradation of HMHP could be a new source of formic acid in the atmosphere. Additionally, the unimolecular decomposition of HMHP is another important removal process in the atmosphere. Chen et al. (2016b) found that the formation of CH_2O and H_2O_2 is more preferable than that of the production of HCOOH and H_2O. Kumar et al. (2014) obtained the same conclusion that the aldehyde- or ketone-forming pathway is kinetically favored over that the carboxylic acid-forming channel in the unimolecular decomposition of a variety of

https://doi.org/10.5194/acp-2021-890
Preprint. Discussion started: 8 November 2021


Atmospheric Chemistry and Physics Discussions

HHPs. All the above milestone investigations offer very useful information for understanding the decomposition of HHPs in the gas phase. However, to the best of our knowledge, there is a few studies on the subsequent transformations of the resulting H-abstraction products formed from the OH-initiated oxidation of larger HHPs. And the effect of the size and number of substituents on the rates and outcomes of SOA precursors (e.g. ROOR, HOMs) is uncertain up to now. Therefore, it is necessary to assess the potential of larger HHPs and their oxidation products to substantial SOA formation under different NO_x conditions.

In this article, we mainly investigate the detailed mechanisms and kinetic properties of distinct HHPs oxidation initiated by OH radical by employing quantum chemical and kinetics modeling methods. For the resulting H-abstraction products RO_2 radicals, the subsequent reactions involving self-reaction, autoxidation and reaction with HO_2 radical are taken into account in the absence of NO, while the subsequent reactions including addition, decomposition and H-abstraction by O_2 are considered in the presence of NO. The investigated HHPs in this work are generated from the bimolecular reactions of distinct carbonyl oxides (CH_2OO, *anti*-CH_3CHOO and $(CH_3)_2COO$) with water vapor. While the product of *syn*-CH_3CHOO reaction with water is not taken into consideration because it mainly proceeds thermal unimolecular decay to OH radical, rather than reaction with water (Zhou et al., 2019).

2. Computational details

2.1 Electronic structure and energy calculations

The equilibrium geometries of all the open-shell species, including reactants (R), pre-reactive complex (RC), transition state (TS), post-reactive complex (PC), and products (P), are fully optimized at the unrestricted M06-2X/6-311+G(2df,2p) level of theory (UM06-2X) (Zhao and Truhlar, 2006; Zheng and Truhlar, 2009), whereas all the closed-shell species are optimized at the restricted M06-2X/6-311+G(2df,2p) level of theory (RM06-2X). This is because the M06-2X functional has been proven to produce reliable performance for describing thermochemistry, kinetics and non-covalent interactions (Zhao and Truhlar, 2008). Moreover, the broken symmetry

https://doi.org/10.5194/acp-2021-890
Preprint. Discussion started: 8 November 2021


Atmospheric Chemistry and Physics Discussions

UM06-2X method is applied to generate the initial guesses of the tetroxide intermediate and transition state geometries with mixed HOMO and LUMO ($S^2 \approx 1$) by using the guess = mix keyword. Previous literatures have been confirmed that the energies obtained from unrestricted DFT are comparable to the multi-reference CASSCF method (Lee et al., 2016; Bach et al., 2005). Harmonic vibrational frequencies are performed at the same level to verify that each stationary point is either a true minima (with no imaginary frequency) or a transition state (with one imaginary frequency). Zero-point vibrational energy (ZPVE) and Gibbs free energies corrections (G_{corr}) from harmonic vibrational frequencies are scaled by a factor of 0.98 (Zhao and Truhlar, 2006). The intrinsic reaction coordinate (IRC) calculations are performed to verify the connection between the transition state and the designated reactant and product (Fukui, et al., 1981). Then, the single-point energies are estimated at the (U/R)M06-2X/ma-TZVP level of theory (Zheng et al., 2011). In order to further evaluate the reliability of the employed method in predicting reaction mechanism, the single-point energies for all stationary points involved in the initiation H-abstraction reactions are recalculated at the (U/R)CCSD(T)/6-311+G(2df,2p) level of theory based on the (U/R)M06-2X optimized geometries. Furthermore, the basis set superposition error (BSSE) is also performed to evaluate the stability of the pre-reactive complexes by employing the counterpoise method (Boys and Bernardi, 1970). For simplicity, no prefix is adopted throughout this article. Herein, the Gibbs free energy (G) for each species is obtained by combining the single-point energy with the Gibbs correction ($G = G_{corr} + E$). The electronic energy ($\Delta E_a^{\#}$) and free energy ($\Delta G_a^{\#}$) barriers are defined as the difference in energy between transition state and pre-reactive complex ($\Delta E_a^{\#} = E_{TS} - E_{RC}$ and $\Delta G_a^{\#} = G_{TS} - G_{RC}$). The reaction free energies (ΔG) is referred to the difference in energy between product and reactant ($\Delta G = G_P - G_R$). The calculated $\Delta E_a^{\#}$ and $\Delta G_a^{\#}$ for the initiation H-abstraction pathways are summarized in Table S1. As shown in Table S1, the mean absolute deviations (MADs) of $\Delta E_a^{\#}$ and $\Delta G_a^{\#}$ between CCSD(T)/6-311+G(2df,2p) and M06-2X/ma-TZVP approaches are 0.35 and 0.33 kcal mol^{-1}, respectively; the largest deviations of $\Delta E_a^{\#}$ and $\Delta G_a^{\#}$ are 0.80 and 0.80 kcal mol^{-1}, respectively. These results

https://doi.org/10.5194/acp-2021-890
Preprint. Discussion started: 8 November 2021


Atmospheric Chemistry and Physics Discussions

reveal that the energies obtained from the M06-2X/ma-TZVP method are in very good accord with those from the gold-standard coupled-cluster approach CCSD(T) within the uncertainties of systematic errors. In order to achieve a balance between the accuracy and computational cost, the M06-2X/ma-TZVP method is selected to investigate the atmospheric degradation of HHP initiated by OH radical under different conditions. In the following sections, unless otherwise stated, the $\Delta G_a^{\#}$ is applied to construct the reaction profiles.

For the H-shift reactions of peroxy radicals (RO_2) in the autoxidation processes, reactants, transition states and products have multiple conformers. Previous literatures have demonstrated that the reaction kinetics of multiconformers involvement are more precisely than that of the single conformer approximation (Møller et al., 2016, 2020). Herein, the multiconformers approximation is performed to investigate the $RO_2\cdot$ autoxidation reactions. A conformer search within the Molclus program is employed to generate a pool of conformers for RO_2 radicals (Lu, 2020). Conformers with relative Gibbs free energies of less than 2.0 kcal mol^{-1} are further optimized at the M06-2X/6-311+G(2df,2p) level of theory, followed by single-point energies calculations at the M06-2X/ma-TZVP level of theory. On the basis of the calculated Gibbs free energies, the Boltzmann populations (w_i) of each $RO_2\cdot$ conformer is expressed as eqn 1.

$$w_i = \frac{e^{-\Delta G_i / k_B T}}{\sum_i e^{-\Delta G_i / k_B T}} \quad (1)$$

where ΔG_i is the relative Gibbs free energy of conformer i, k_B is the Boltzmann's constant, T is temperature in Kelvin. All the quantum chemical calculations are performed by using the Gaussian 09 program package (Frisch et al., 2009).

2.2 Kinetics calculations

The rate coefficients of bimolecular reactions are calculated by using the Rice-Ramsperger-Kassel-Marcus theory coupled with energy-grained master equation (RRKM-ME) method (Holbrook et al., 1996), and the rate coefficients of $RO_2\cdot$ autoxidation reactions are determined by employing the multiconformer

https://doi.org/10.5194/acp-2021-890
Preprint. Discussion started: 8 November 2021


Atmospheric Chemistry and Physics Discussions

196 transition state theory (MC-TST) approach (Møller et al., 2016). The RRKM-ME and
197 MC-TST calculations are performed by implementing the MESMER 6.0 program
198 suite (Glowacki et al., 2012). N_2 is used as the buffer gas. The single exponential
199 down model is employed to simulate the collision energy transfer ($<\Delta E>_{down}$ = 200
200 cm^{-1}). The collisional Lennard-Jones parameters are estimated by using an empirical
201 formula described by Gilbert and Smith (1990). The MC-TST rate coefficient $k_{MC\text{-}TST}$
202 is calculated by the sum of the individual intrinsic reaction coordinate TST (IRC-TST)
203 rate coefficient $k_{IRC\text{-}TST}$, each weighted by Boltzmann population of corresponding
204 RO_2 ·conformer (Møller et al., 2016).

205 $$k_{MC\text{-}TST} = \sum_{i}^{\text{all TS conf.}} w_i \times k_{IRC\text{-}TST i} \quad (2)$$

206 where $k_{IRC\text{-}TST i}$ represents the rate coefficient of conformer i, and w_i is the relative
207 Boltzmann population of the corresponding reactant connected to TS_i. The
208 one-dimensional asymmetry Eckart model is employed to calculate the tunneling
209 correction (Eckart, 1930). Considering that the uncertainty in barrier heights (~ 1.0
210 kcal·mol^{-1} by the M06-2X method) and in tunneling corrections, the uncertainty of the
211 calculated rate coefficient is within one order of magnitude in the present study.

212 ## 3. Results and discussion

213 ### 3.1 Initiation reaction of HHPs with OH radical

214 Previous literatures have proposed that the lifetime of CI with respect to the
215 reaction with water vapour exhibits a highly dependent on the nature of CIs (Anglada
216 and Solé, 2016; Taatjes, et al., 2013; Anglada, et al., 2011), and the primary product is
217 HHPs in both gas phase and air/water interface (Chao et al., 2015; Chen et al., 2016a;
218 Smith, et al., 2015; Zhu, et al., 2016; Zhong, et al., 2018). In the present study, we
219 mainly consider three kinds of HHPs originated from the addition of water to CH_2OO
220 and methyl-substituted CI (*anti*-CH_3CHOO and $(CH_3)_2COO$). The formed HHPs have
221 several conformations differing in the relative spatial orientation of hydrogen atoms
222 involved in both -OOH and -OH moieties. The unique conformation with the lowest
223 energy is identified as the global minimum to investigate its degradation mechanism.

https://doi.org/10.5194/acp-2021-890
Preprint. Discussion started: 8 November 2021


Atmospheric Chemistry and Physics Discussions

The formed HHPs possess -CH_3, -CH_2-, -OH and -OOH functional groups as displayed in Figure 1. The unimolecular dissociation is not taken into account in this study due to their extremely high barriers (~ 45 kcal mol^{-1}) (Kumar et al., 2014; Chen, et al., 2016b). Considering the different chemical environments of hydrogen atoms, the atmospheric transformation of HHPs initiated by OH radical should have four types of H-abstraction pathways as presented in Figure 2. Labels A, B, C, and D represent the relative free energies of RC, TS, PC and P. R1 and R2 stand for the positions of -H and -CH_3 groups, respectively. As shown in Figure 2, each H-abstraction reaction begins with the formation of a RC in the entrance channel, then it immediately transforms into the respective product via the corresponding transition state. The $\Delta G_a^{\#}$ and ΔG for every elementary reaction included in initiation reactions of OH radical with distinct HHPs are summarized in Table 1. As shown in Table 1, for the H-abstraction reactions of OH radical with $HOCH_2OOH$, the $\Delta G_a^{\#}$ are reduced in the order of 6.4 (R1) > 5.8 (R3) > 5.1 (R2) > 1.5 (R4) kcal mol^{-1}, indicating that H-abstraction from the -OOH group is the most favourable. One reason for the barrier difference could lie in the fact that the bond dissociation energies (BDE) of different types of bonds are significantly different in the $HOCH_2OOH$ molecule. The BDE are decreased in the order of 103.7 (O_1-H_1) > 98.2 (C_1-H_2) > 97.4 (C_1-H_1) > 87.2 (O_3-H_2) kcal mol^{-1}, which are in good agreement with the order of barrier heights. As indicated by their ΔG values, it can be found that the exothermicity of R4 is the largest among these four H-abstraction reactions. This phenomenon might be ascribed to the resonance stabilization of the formed peroxy radical $HOCH_2OO$. It is concluded that H-abstraction from the -OOH group resulting in formation of $HOCH_2OO$ radical is the dominant pathway. Similar conclusions are also derived from the reactions of OH radical with both $HOCH_3CHOOH$ and $HO(CH_3)_2COOH$ that the H-abstraction from the -OOH group is preferable on both thermodynamically and kinetically. It is worth noting that the barrier of dominant pathway is increased as the number of methyl group is increased.

For the initiation reactions of distinct HHPs with OH radical, the rate coefficients of every H-abstraction pathway and their branching ratios (Γ) are estimated over the

https://doi.org/10.5194/acp-2021-890
Preprint. Discussion started: 8 November 2021


Atmospheric Chemistry and Physics Discussions

temperature range from 273 to 400 K as summarized in Table S2-S4. As shown in Table S2, the total rate coefficients k_{tot} decrease in the range of 4.8×10^{-11} (273 K) to 7.6×10^{-12} (400 K) cm^3 $molecule^{-1}$ s^{-1} with the temperature increasing, and they exhibit a marked negative temperature dependence. At ambient temperature, the rate coefficient is calculated to be 3.2×10^{-11} cm^3 $molecule^{-1}$ s^{-1}, which is a factor of 3.7 higher than the experimental value ($(7.1 \pm 1.5) \times 10^{-12}$ cm^3 $molecule^{-1}$ s^{-1}) (Allen et al., 2018). Such a discrepancy is might be due to uncertainties in the barrier height and tunneling correction. The calculated $k_{R4(O3\text{-}H2)}$ is almost identical to the k_{tot} in the whole temperature range, which are 1-2 orders of magnitude greater than those of $k_{R1(O1\text{-}H1)}$, $k_{R2(C1\text{-}H1)}$ and $k_{R3(C1\text{-}H2)}$. The result shows that H-abstraction by OH radical from the -OOH group resulting in formation of peroxy radical is preferable kinetically. Similarly, $\Gamma_{R4(O3\text{-}H2)}$ is overwhelmingly greater than those of $\Gamma_{R1(O1\text{-}H1)}$, $\Gamma_{R2(C1\text{-}H1)}$ and $\Gamma_{R3(C1\text{-}H2)}$ in the entire temperature range, and it exhibits a negative T-dependence. $\Gamma_{R1(O1\text{-}H1)}$, $\Gamma_{R2(C1\text{-}H1)}$ and $\Gamma_{R3(C1\text{-}H2)}$ are less than 8% at 273-400 K, indicating that these three kinds of H-abstraction pathways are of minor importance. Similar conclusion is also derived from the reactions of OH radical with HO-CH(CH_3)OOH and HO-C(CH_3)$_2$OOH that H-abstraction from the -OOH group is predominant (Table S3 and S4). It is worth mentioning that the dimethyl substitutions decrease the branching ratio of dominant pathway and increase the branching ratio of H-abstraction pathway from -OH group. Compared to the rate coefficient of dominant pathway in the parent system, it is almost identical when a methyl group substitution occurs at the C_1-position, whereas it reduces by a factor of ~5 when two methyl groups introduce into the C_1-position. For example, at room temperature, $k_{R4(O3\text{-}H2)}$ is estimated to be 2.9×10^{-11} cm^3 $molecule^{-1}$ s^{-1}, which is greater than the corresponding values of $k_{R4'(O3\text{-}H2)}$ (2.8×10^{-11}) and $k_{R4''(O3\text{-}H2)}$ (5.4×10^{-12}) by 1.0 and 5.4 times.

3.2 Subsequent reactions of H-abstraction products RO_2 radicals in pristine environment

In principle, the H-abstraction products RO_2 radicals have three types of channels in pristine environment: (1) the self-reactions of RO_2 radicals firstly produce

https://doi.org/10.5194/acp-2021-890
Preprint. Discussion started: 8 November 2021


Atmospheric Chemistry and Physics Discussions

tetroxide intermediates, followed by homolytic cleavage of two external O-O bonds to generate RO ·+ O_2 (propagation channel), or via hydrogen transfer to give carbonyl + alcohol + O_2 or through the O-O bond forming to produce dimer ROOR + O_2 (Zhang et al., 2012; Atkinson and Arey, 2003) (termination channel) that has been recognized as an important SOA precursor (Valiev et al., 2019; Hasan et al., 2020); (2) RO_2 radicals react with HO_2 radical leading to the formation of hydroperoxide ROOH, alcohol, OH and other products (Winiberg et al., 2016; Chen et al., 2021); (3) RO_2 radicals autoxidation through intramolecular H-shift and alternating O_2 addition steps generate HOMs that have low vapor pressure, low volatility and highly oxygenated compounds contributing substantially to the formation and growth of organic aerosol (Ehn et al., 2014; Bianchi et al., 2019; Nozière and Vereecken, 2019; Rissanen et al., 2014). The relevant details for these three kinds of reactions will be discussed in the following paragraph.

3.2.1 Reactions mechanism for the self-reaction of RO_2 radicals

The self-reaction is one of dominant decay pathways for RO_2 radicals when the concentration of NO is low. The self-reaction of RO_2 radicals usually follows the Russell mechanism (Russell, 1957), and mainly includes four kinds of channels: (1) $2RO_2 \cdot \rightarrow 2RO \cdot + O_2$; (2) $2RO_2 \cdot \rightarrow ROH + RCO + O_2$; (3) $2RO_2 \cdot \rightarrow ROOR + O_2$; (4) $2RO_2 \cdot \rightarrow ROOH + R'CHOO$ (Atkinson and Arey, 2003). The relative importance of different channels varies strongly depending on the conformation, size and complexity of RO_2 radicals (Iyer et al., 2018; Lee et al., 2016). A schematic potential energy surface (PES) for the self-reaction of $HOCH_2OO$ radical is drawn in Figure 3. From Figure 3, it is seen that the tetroxide complexes IM1-a and IM2-a are formed by a head-to-head interaction (the O_3-O_6 bond forming), which lie 2.9 and 3.4 kcal·mol^{-1} above the initial two $HOCH_2OO$ radicals in energy. Then IM1-a fragments into dimer S1 + $^1O_2$ via the dissociation of both O_2-O_3 and O_5-O_6 bonds and the formation of O_2-O_5 bond with the barrier of 43.3 kcal·mol^{-1}. IM2-a leads to $HOCH_2OOH$ + HOCHOO (CI) through the cleavage of both O_3-O_6 and C_2-H_5 bonds and the formation of O_3-H_5 bond with the barrier of 51.5 kcal·mol^{-1}. But the barriers are

https://doi.org/10.5194/acp-2021-890
Preprint. Discussion started: 8 November 2021


Atmospheric Chemistry and Physics Discussions

312 comparatively high, making these two pathways slow. Alternatively, the self-reaction
313 also leads to the formation of tetroxide intermediate S2 via oxygen-to-oxygen
314 coupling transition state TS3 with the electronic energy and free energy barriers of 7.3
315 and 19.6 kcal $\cdot$mol^{-1}. Kumar and Francisco reported that the electronic energy barrier
316 of the gas phase decomposition of $HOCH_2OO$ radical is 14.0 kcal $\cdot$mol^{-1} and it could
317 be a new source of HO_2 radical in the troposphere (Kumar and Francisco, 2015). It is
318 interesting to compare the barriers of unimolecular decomposition and self-reaction of
319 $HOCH_2OO$ radical, it can be found that the self-reaction leading to the formation of
320 tetroxide intermediate S2 is significantly feasible.

321 S2 can either dissociate $HOCH_2O$; HCOOH and $HO_2\cdot$ via an hydrogen transfer
322 and the cleavage of both O_2-O_3 and O_5-O_6 bonds with the barrier of 29.8 kcal $\cdot$mol^{-1},
323 or generate caged tetroxide intermediate S4 through the asymmetric O_2-O_3 and O_5-O_6
324 bonds cleavage with the barriers of 19.1 and 3.1 kcal $\cdot$mol^{-1}, respectively. The latter
325 pathway is more preferable than the former channel owing to its lower barrier. The
326 overall spin multiplicity of S4 is singlet, in which the O_2 moiety maintains the triplet
327 ground state and is very loosely bound. In order to preserve the overall singlet
328 multiplicity, the two $HOCH_2O$ radical pairs (^{3}($HOCH_2O\cdots HOCH_2O$)) must have the
329 triplet multiplicity. S4 could be regarded as the ground-state $^3O_2$ moving away from
330 the two $HOCH_2O$ radical pairs that keep interacting. Due to the difficulty in
331 performing the constrained optimization for the dissociation of S4, the $^3O_2$ moiety is
332 considered as a leaving moiety away from two $HOCH_2O$ radical pairs, and merely the
333 dissociation of ^{3}($HOCH_2O\cdots HOCH_2O$) is taken into consideration in the present
334 study. It has three types of pathways: (1) it yields $HOCH_2OH$ and excited-state
335 ^{3}HCOOH through the hydrogen transfer step with the barrier of 14.0 kcal $\cdot$mol^{-1} and
336 10.2 kcal $\cdot$mol^{-1} exothermicity, followed by the excited ^{3}HCOOH to go back to the
337 ground-state ^{1}HCOOH; (2) it generates two $HOCH_2O$ radicals via the barrierless
338 process with 16.9 kcal $\cdot$mol^{-1} exothermicity; (3) it produces dimer S5 via an
339 intersystem crossing (ISC) step with 32.1 kcal $\cdot$mol^{-1} exothermicity. Based on the
340 calculated reaction barriers, it can be found that the rate-limiting step is the scission of
341 O_2-O_3 bond (R5) in the unimolecular decomposition of S2. This conclusion coincides

https://doi.org/10.5194/acp-2021-890
Preprint. Discussion started: 8 November 2021


Atmospheric Chemistry and Physics Discussions

with the previous result obtained from the dissociation of di-t-butyl tetroxide that the rate-controlling step is the rupture of single O-O bond (Lee et al., 2016). Valiev et al. proposed that the ISC rate of ROOR dimer formed from the different (RO ··R'O) systems is extremely rapid (> 10^8 s^{-1}) and exhibits a strong stereoselectivity (Valiev et al., 2019).

As shown in Figure 4, the dominant pathway for the self-reaction of $HOCH_3CHOO$ radical begins with the formation of tetroxide intermediate S7 via an oxygen-to-oxygen coupling transition state TS10 with the barrier of 19.9 kcal mol^{-1}; then it transforms into the caged tetroxide intermediate S9 of overall singlet spin multiplicity through the asymmetric two-step O-O bond cleavage with the barriers of 21.4 and 1.3 kcal mol^{-1}; finally, S9 decomposes into the propagation (two $HOCH_3CHO$ radical) and termination products ($HOCH_3CHOH$ + $^3CH_3OOH$ and dimer S10) with the exothermicity of 12.5, 11.7 and 33.0 kcal mol^{-1}, with respect to the initial two $HOCH_3CHOO$ radicals. The rate-determining step is the scission of O_2-O_3 bond (R12) in the dissociation processes of S7. This result is consistent with the above-mentioned conclusion derived from the decomposition of S2 in the self-reaction of $HOCH_2OO$ radical. The detailed mechanism for the self-reaction of $HO(CH_3)_2COO$ radical is quite similar to that of the $HOCH_2OO$ and $HOCH_3CHOO$ radicals systems (Figure 5), and is not discussed in detail to avoid redundancy. It is worth noting that the termination products are not found in the $HO(CH_3)_2COO$ radical reaction system owing to the absence of alpha hydrogen atom. Compared to the barrier of rate-determining route R5 in the parent system, the barrier of rate-limiting step R17 is increased by about 5.0 kcal mol^{-1} when two methyl substitutions introduce at the C1-position. The reason might be attributed to the cage escape of alkoxyl radicals. It is therefore that the tertiary RO_2 radicals have great opportunity to react with HO_2 radical or autoxidation in pristine environment.

3.2.2 Reactions mechanism for the reaction of RO_2 with HO_2 radical

When NO is present in low concentration, the bimolecular reaction of RO_2 radical with HO_2 radical is generally expected to be the dominant pathway as the main

https://doi.org/10.5194/acp-2021-890
Preprint. Discussion started: 8 November 2021


Atmospheric Chemistry and Physics Discussions

product hydroperoxide ROOH. The main primary sources of HO_2 radical in the atmosphere are from the photolysis of CH_2O and OVOCs, and the ozonolysis reactions (Stone et al., 2012; Hofzumahaus et al., 2009). The typical atmospheric concentrations of HO_2 radical are 5, 20 and 50 pptv in the urban, rural and forest environments (Bianchi et al., 2019). A schematic PES for the reactions of HO_2 radical with distinct RO_2 radicals is presented in Figure 6. As shown in Figure 6, the bimolecular reaction between $HOCH_2OO\cdot$ and $HO_2\cdot$ starts with the formation of IM19-a in the entrance channel, which is higher in energy than the separate reactants 3.8 kcal mol^{-1}. Then it transforms into $HOCH_2OOH$ via the hydrogen transfer step with the barrier of 2.0 kcal mol^{-1}. The overall reaction is strongly exothermic and spontaneous, indicating that it is feasible in the atmosphere. Similar phenomenon is also observed from the bimolecular reactions of $HOCH_3CHOO$ and $HO(CH_3)_2COO$ with HO_2 radicals. Compared to the barrier of parent system, it is only reduced by 0.1 kcal mol^{-1} when one or two methyl substitutions occur at the C1-position. This result implies that the barrier height is not seem to be influenced by the number of methyl substitution. The rate coefficients of distinct RO_2 radicals reactions with HO_2 radical are summarized in Table S5. As shown in Table S5, the rate coefficient of $HOCH_2OO\cdot$ reaction with $HO_2\cdot$ (R19) varies from 3.1×10^{-11} (273 K) to 2.1×10^{-12} cm^3 $molecule^{-1}$ s^{-1} (400 K), and they exhibit a negative temperature dependence. At room temperature, the rate coefficient is estimated to be 1.7×10^{-11} cm^3 $molecule^{-1}$ s^{-1}, translating into the pseudo-first-order rate constants $k'_{HO2} = k_{HO2}[HO_2]$ of 1.1×10^{-3}, 4.2×10^{-3} and 1.1×10^{-2} s^{-1}, respectively, in the urban, rural and forest environments. Compared to the rate coefficient of parent system, it is increased by a factor of 3-5 when one or two methyl groups introduce into the C1-position. The pseudo-first-order rate constants of $HOCH_3CHOO\cdot + HO_2\cdot$ (R20) and $HO(CH_3)_2COO\cdot + HO_2\cdot$ (R21) are 2.9×10^{-2} and 4.6×10^{-2} s^{-1} in the forest environments.

3.2.3 Reactions mechanism for the autoxidation of RO_2 radicals

Autoxidation of RO_2 radical is known to play an important role in the (re)generation of HO_x radicals and in the formation of HOMs (Wang et al., 2017;

https://doi.org/10.5194/acp-2021-890
Preprint. Discussion started: 8 November 2021


Atmospheric Chemistry and Physics Discussions

Bianchi et al., 2019; Rissanen et al., 2014; Ehn et al., 2017). The detailed mechanism includes an intramolecular H-atom migration from the -CH_3 or -CH_2- groups to the -OO · group, resulting in formation of hydroperoxyalkyl radicals QOOH, followed by O_2 addition to form a new peroxy radical ($HOOQO_2$), one after the other, and the resulting finally HOMs (Nozière and Vereecken, 2019; Vereecken and Nozière, 2020). For the autoxidation of $HOCH_2OO$ radical, reactants, transition states and products have multiple conformers due to the effect of degree of freedom for internal rotation. Based on the conformer search results, it can be found that the $HOCH_2OO$ radical has four energetically similar conformers ($HOCH_2OO$-a, $HOCH_2OO$-b, $HOCH_2OO$-c and $HOCH_2OO$-d). The relative free energy and Boltzmann population (w_i) of individual conformer are listed in Table S6. As shown in Table S6, the Boltzmann populations of these four conformers are predicted to be 46.39, 46.31, 2.99 and 4.32%, respectively. It deserves mentioning that the conformers $HOCH_2OO$-c and $HOCH_2OO$-d are not proceed H-shift reactions.

A schematic PES for the H-shift reactions of conformers $HOCH_2OO$-a and $HOCH_2OO$-b is drawn in Figure 7. As can be seen in Figure 7, all H-shift reactions are strongly endergonic (> 12.4 kcal·mol^{-1}), implying that they are unfavorable thermodynamically. For the lowest-energy conformer $HOCH_2OO$-a, a 1,3-H shift from the -CH_2 group to the terminal oxygen leads to the formation of S16-a (HO·CHOOH) with the barrier of 41.6 kcal·mol^{-1}. Similarly, $HOCH_2OO$-b also can isomerize to S16-b1 and S16-b2 via the four-membered ring transition states TS22-b1 and TS22-b2 (1,3-H shifts) with the barriers of 41.6 and 45.0 kcal·mol^{-1}. These three H-shift reactions have comparatively high barrier, making them irrelevant under atmospheric conditions. The high barriers of 1,3-H shifts can be interpreted as the result of the large ring strain energy (RSE) in the cyclic transition state geometries. $k_{IRC\text{-}TST}$ and $k_{MC\text{-}TST}$ are estimated over the temperature range of 273-400 K as listed in Table S7. From Table S7, it can be seen that $k_{IRC\text{-}TST}$ and $k_{MC\text{-}TST}$ are significantly increased with rising temperature, and they exhibit a marked positive temperature dependence. This result implies that the temperature increasing is beneficial to the occurrence of autoxidation reactions. Compared to the rate coefficients of 1,5- and

https://doi.org/10.5194/acp-2021-890
Preprint. Discussion started: 8 November 2021


Atmospheric Chemistry and Physics Discussions

1,6-H shifts in aliphatic RO_2 radicals (~ 10^{-6} s^{-1}) (Vereecken and Nozière, 2020), it can be found that $k_{IRC\text{-}TST}$ of 1,3-H shifts in $HOCH_2OO$ radical are several orders of magnitude lower than that of the former case. Similar conclusion is also derived from the autoxidation of $HOCH_3CHOO$ and $HO(CH_3)_2COO$ radicals that 1,3- and 1,4-H shifts are of less importance in the atmosphere owing to their extremely high barrier (Figure S1 and S2). In order to avoid redundancy, we will not discuss the autoxidation mechanism and kinetics of $HOCH_3CHOO$ and $HO(CH_3)_2COO$ radicals in the present study (Table S8-S11). It is worth mentioning that the $k_{MC\text{-}TST}$ is significantly increased as the number of methyl group is increased. For example, the room temperature $k_{MC\text{-}TST}$ of $HOCH_2OO$ radical autoxidation is calculated to be 4.4×10^{-16} s^{-1}, which is about a factor of 660 and 6820 lower than those of the $HOCH_3CHOO$ (2.9×10^{-13} s^{-1}) and $HO(CH_3)_2COO$ (3.0×10^{-12} s^{-1}) radicals autoxidation.

3.3 Subsequent reactions of H-abstraction products RO_2 radicals in urban environments

NO_x are present in high concentration in urban environments, reaction with NO is the dominant chemical sink for RO_2 radicals leading to the formation of NO_2, RO radicals, organic nitrate, etc. (Atkinson and Arey, 2003; Orlando and Tyndall, 2012; Perring et al., 2013) The formation of NO_2 through subsequent photolysis (λ < 420 nm) produces ozone and NO, increasing the concentrations of near-surface ozone and propagating NO_x chain (Orlando and Tyndall, 2012). The production of RO radical can either fragment into small molecules via β-site C-C bond scission, or generate aldehyde and HO_2 radical through hydrogen abstraction by O_2 (if an alpha hydrogen is present), or transform into HOMs through consecutive intramolecular H-shift and O_2-addition routes (if feasible) (Chen et al., 2021; Rissanen et al., 2014; Aschmann et al., 2000). The relative importance of different pathways is highly dependent on the nature of R group (Nozière and Vereecken, 2019; Aschmann et al., 2000). The schematic PES for the reactions of distinct RO_2 radicals with NO are displayed in Figure 8-10. As shown in Figure 8, the bimolecular reaction between $HOCH_2OO$ radical and NO initially leads to nitrite adduct S19 via the barrierless addition of NO

https://doi.org/10.5194/acp-2021-890
Preprint. Discussion started: 8 November 2021


Atmospheric Chemistry and Physics Discussions

459 to terminal oxygen O_3 of $HOCH_2OO$ radical. The formed S19 exists two isomers:
460 S19-*cis* refers to the O_2 and O_4 on the same side ($DO_2O_3N_1O_4$ = 2.3 °), whereas
461 S19-*trans* refers to the O_2 and O_4 on the opposite side ($DO_2O_3N_1O_4$ = -179.8 °) with
462 respect to the O_3-N_1 bond. The calculations show that S19-*cis* is more stable than that
463 of the S19-*trans* by 1.1 kcal·mol^{-1} in energy. The tautomerization between S19-*cis*
464 and S19-*trans* proceeds through the rotating of O_3-N_1 bond with the barrier of 14.4
465 kcal·mol^{-1}, implying that they can be regarded as the separate atmospheric species.
466 According to the Boltzmann-weighted distribution, at room temperature, the predicted
467 percentages of S19-*cis* and S19-*trans* are 86.5% and 13.5%, respectively. The result
468 implies that the dominant product of $HOCH_2OO$ radical reaction with NO is S19-*cis*,
469 and it is selected as a model compound to insight into the mechanism of secondary
470 reactions in the following sections.

471 S19-*cis* can either isomerize to organic nitrate S20 ($HOCH_2NO_2$) via the O_2-O_3
472 bond breaking and O_2-N_1 bond forming with the barrier of 47.8 kcal·mol^{-1}, or
473 decompose into $HOCH_2O$ radical and NO_2 via the cleavage of O_2-O_3 bond with the
474 barrier of 11.3 kcal·mol^{-1}. The result shows that the latter pathway is more favor than
475 the former channel due to its lower barrier. It should be noted that the corresponding
476 transition state TS27 is not located using M06-2X functional, but it is located at the
477 MP2/6-311+G(2df,2p) level of theory and is verified using IRC calculations. The
478 formed $HOCH_2O$ radical has two kinds of pathways: (1) it directly decomposes into
479 CH_2O and OH radical via β-site C_1-O_1 bond scission with the barrier of 52.4
480 kcal·mol^{-1}; (2) it undergoes hydrogen abstraction by O_2 to produce HCOOH and HO_2
481 radical with the barrier of 26.4 kcal·mol^{-1}. Based on the above discussions, it is
482 concluded that the rate-limiting step is the hydrogen abstraction pathway R29 of the
483 whole $HOCH_2OO$ + NO reaction.

484 The bimolecular reaction of $HOCH_3CHOO$ radical with NO has similar
485 pathways (Figure 9). It firstly transforms to S21-*cis* via the barrierless addition with
486 the binding energy of 13.1 kcal·mol^{-1}; secondly, S21-*cis* fragments into $HOCH_3CHO$
487 radical and NO_2 with the barrier of 11.5 kcal·mol^{-1}; finally, $HOCH_3CHO$ radical
488 primarily dissociates to HCOOH and CH_3 radical with the barrier of 8.3 kcal·mol^{-1}.

https://doi.org/10.5194/acp-2021-890
Preprint. Discussion started: 8 November 2021


Atmospheric Chemistry and Physics Discussions

The rate-determining step is the O_2-O_3 bond scission of the overall $HOCH_3CHOO$ + NO reaction. Compared to the decomposition of $HOCH_2O$ radical, the dominant pathway becomes the β-site C-C bond scission when a methyl group substitution occurs at the C_1-position. Similar conclusion is also obtained from the bimolecular reaction of $HO(CH_3)_2COO$ with NO that the decomposition of $HO(CH_3)_2CO$ radical resulting in formation of CH_3COOH and CH_3 radical is the most feasible channel (Figure 10). These conclusions are further supported by the previous experimental result that β-hydroxy intermediates primarily proceed decomposition rather than react with O_2 in the presence of NO (Aschmann et al., 2000).

The rate coefficients of dominant pathways in the $HOCH_2OO\cdot$ + NO, $HOCH_3CHOO\cdot$ + NO and $HO(CH_3)_2CHOO\cdot$ + NO reactions are listed in Table S12-14. As shown in Table S12, k_{R27} vary slightly form 5.1×10^{-12} (273 K) to 1.3×10^{-12} (400 K) cm^3 $molecule^{-1}$ s^{-1}, and they exhibit a weakly negative temperature dependence. At ambient temperature, k_{R27} is calculated to be 4.3×10^{-12} cm^3 $molecule^{-1}$ s^{-1}, which agrees well with the values of 8.5×10^{-12} cm^3 $molecule^{-1}$ s^{-1} obtained from the typical $RO_2\cdot$ + NO reactions (Bianchi et al., 2019). The typical atmospheric concentrations of NO are about 10 ppbv, 1 ppbv and 20 pptv in the urban, rural and forest environments (Bianchi et al., 2019), resulting in the pseudo-first-order rate constants $k'_{NO} = k_{NO}[NO]$ of 6.5×10^{-1}, 6.5×10^{-2}, and 1.3×10^{-3}, respectively. It is of interest to assess the relative importance for the autoxidation of $HOCH_2OO$ radical and bimolecular reactions with $HO_2\cdot$ and NO based on the calculated $k_{MC\text{-}TST}$, k'_{HO2} and k'_{NO}. It can be found that the $HOCH_2OO$ radical autoxidation are of less importance, the HO_2 radical reaction is favorable in the forest environment, while the NO reaction is predominant in the urban and rural regions. Similar conclusion is also obtained from the cases of $HOCH_3CHOO$ and $HO(CH_3)_2CHOO$ radicals.

4. Conclusions

The detailed mechanisms and kinetic properties of OH-initiated oxidation of distinct HHPs and subsequent transformation of resulting H-abstraction products are investigated using quantum chemical and kinetics modeling methods. The main

https://doi.org/10.5194/acp-2021-890
Preprint. Discussion started: 8 November 2021


Atmospheric Chemistry and Physics Discussions

conclusion are summarized as follows:

(a) The H-abstraction by OH radical from the -OOH group of distinct HHPs leading to the formation of RO_2 radicals is preferable, and the barrier of dominant pathway is increased as the number of methyl group is increased. Compared to the rate coefficient of dominant pathway in the parent system, it is almost identical when a methyl group substitution occurs at the C_1-position, whereas it reduces by about one order of magnitude when two methyl groups introduce into the C_1-position of $HOCH_2OO$ radical.

(b) The self-reaction of H-abstraction product RO_2 radical initially produces tetroxide intermediate via a head-to-head interaction, then it decomposes into propagation and termination products through the asymmetric two-step O-O bond scission. The rate-limiting step is the first O-O bond cleavage, and the barrier is increased with increasing the number of methyl group.

(c) The bimolecular reactions of distinct RO_2 radicals with HO_2 radical lead to the formation of hydroperoxide ROOH as the main product, and the barrier height is independent on the number of methyl substitution. The calculated rate coefficients exhibit a slightly negative temperature dependence, translating into the pseudo-first-order rate constant k'_{HO2} of ~ 10^{-2} s^{-1} in the forest environments.

(d) The autoxidations of RO_2 radicals involved in the present system are of less importance in the atmosphere because the rate-limiting H-shift steps have dramatically high barriers and strongly endergonic. The calculated $k_{MC\text{-}TST}$ is significantly increased as the number of methyl group is increased.

(e) The rate-limiting step is the hydrogen abstraction by O_2 in the processes of $HOCH_2OO$ radical reaction with NO, while it becomes the O-O bond scission when one or two methyl substitutions occur at the C1-position of $HOCH_2OO$ radical.

Data availability.

The data are accessible by contacting the corresponding author (huangyu@ieecas.cn).

https://doi.org/10.5194/acp-2021-890
Preprint. Discussion started: 8 November 2021

Atmospheric Chemistry and Physics Discussions

Supplement

Y//X (Y = M06-2X, CCSD(T), X = 6-311+G(2df,2p), ma-TZVP) calculated energy barrier ($\Delta E_a^{\#}$, $\Delta G_a^{\#}$) for OH + HHPs reactions; Rate coefficients of every elementary pathway and their branching ratios (Γ) involved in the initial reactions of OH radical with $HOCH_2OOH$, $HOCH_3CHOOH$ and $HO(CH_3)_2COOH$; Rate coefficients of HO_2 radical reactions with $HOCH_2OO$, $HOCH_3CHOO$ and $HO(CH_3)_2COO$ radicals; The relative free energy and Boltzmann populations (w_i) of the conformer of $HOCH_2OO$, $HOCH_3CHOO$ and $HO(CH_3)_2COO$ radicals; The single-conformer rate coefficients ($k_{IRC\text{-}TST}$) and multi-conformer rate coefficients ($k_{MC\text{-}TST}$) of $HOCH_2OO$, $HOCH_3CHOO$ and $HO(CH_3)_2COO$ radicals; Rate coefficients of dominant pathways in the $HOCH_2OO\cdot$ + NO, $HOCH_3CHOO\cdot$ + NO and $HO(CH_3)_2CHOO\cdot$ + NO reactions; PES ($\Delta G_a^{\#}$ and $\Delta E_a^{\#}$, in italics) for the autoxidation of $HOCH_3CHOO$ and $HO(CH_3)_2COO$ radicals.

Author contributions

LC designed the study. LC and YH wrote the paper. LC performed theoretical calculation. YX, ZJ, and WW analyzed the data. All authors reviewed and commented on the paper.

Conflicts of interest

The authors declare that they have no conflict of interest.

Acknowledgments

This work was supported by the National Natural Science Foundation of China (grant Nos. 42175134, 41805107, and 22002080). Strategic Priority Research Program of the Chinese Academy of Sciences, China (grant Nos. XDA23010300 and

https://doi.org/10.5194/acp-2021-890
Preprint. Discussion started: 8 November 2021

XDA23010000), CAS "Light of West China" Program (XAB2019B01) and the General Project of Shaanxi Province (2020JQ-432).

References

Allen, H. M., Crounse, J. D., Bates, K. H., Teng, A. P., Krawiec-Thayer, M. P., Rivera-Rios, J. C., Keutsch, F. N., Clair, J. M. S., Hanisco, T. F., Møller, K. H., Kjaergaard, H. G., and Wennberg, P. O.: Kinetics and product yields of the OH initiated oxidation of hydroxymethyl hydroperoxide, J. Phys. Chem. A, 122, 6292-6302, https://doi.org/10.1021/acs.jpca.8b04577, 2018.

Anglada, J. M., and Solé, A.: Impact of the water dimer on the atmospheric reactivity of carbonyl oxides, Phys. Chem. Chem. Phys., 18, 17698-17712, http://dx.doi.org/10.1039/C6CP02531E, 2016.

Anglada, J. M., González, J., and Torrent-Sucarrat, M.: Effects of the substituents on the reactivity of carbonyl oxides. A theoretical study on the reaction of substituted carbonyl oxides with water, Phys. Chem. Chem. Phys., 13, 13034-13045, https://doi.org/10.1039/c1cp20872a, 2011.

Aschmann, S. M., Arey, J., and Atkinson, R.: Formation of β-hydroxycarbonyls from the OH radical-initiated reactions of selected alkenes, Environ. Sci. Technol., 34, 1702-1706, https://doi.org/10.1021/es991125a, 2000.

Atkinson, R., and Arey, J.: Atmospheric degradation of volatile organic compounds, Chem. Rev., 103, 4605-4638, https://doi.org/10.1021/cr0206420, 2003.

Bach, R. D., Dmitrenko, O., and Estévez, C. M.: Chemical behavior of the biradicaloid (HO ··ONO) singlet states of peroxynitrous acid. the oxidation of hydrocarbons, sulfides, and selenides, J. Am. Chem. Soc., 127, 3140-3155, https://doi.org/10.1021/ja044245d, 2005.

Berndt, T., Scholz, W., Mentler, B., Fischer, L., Herrmann, H., Kulmala, M., and Hansel, A.: Accretion product formation from self- and cross-reactions of RO_2 radicals in the atmosphere, Angew. Chem. Int. Ed., 57, 3820-3824, https://doi.org/10.1002/anie.201710989, 2018.

Bianchi, F., Kurten, T., Riva, M., Mohr, C., Rissanen, M. P., Roldin, P., Berndt, T., Crounse, J. D., Wennberg, P. O., Mentel, T. F., Wildt, J., Junninen, H., Jokinen, T., Kulmala, M., Worsnop, D. R., Thornton, J. A., Donahue, N., Kjaergaard, H. G., and Ehn, M.: Highly oxygenated organic molecules (HOM) from gas-phase autoxidation involving peroxy radicals: a key contributor to atmospheric aerosol, Chem. Rev., 119, 3472-3509, https://doi.org/10.1021/acs.chemrev.8b00395, 2019,

Boys, S. F., and Bernardi, F.: The calculation of small molecular interactions by the differences of separate total energies. Some procedures with reduced errors, Mol. Phys., 19, 553-566, https://doi.org/10.1080/00268977000101561, 1970.

Chao, W., Hsieh, J. T., Chang, C. H., and Lin, J. J. M.: Direct kinetic measurement of the reaction of the simplest Criegee intermediate with water vapor, Science, 347, 751-754, https://doi.org/10.1126/science.1261549, 2015.

Chen, L., Huang, Y., Xue, Y., Cao, J., and Wang, W.: Competition between HO_2 and H_2O_2 reactions with CH_2OO/*anti*-CH_3CHOO in the oligomer formation: a theoretical perspective, J. Phys. Chem. A, 121, 6981-6991, https://doi.org/10.1021/acs.jpca.7b05951, 2017.

https://doi.org/10.5194/acp-2021-890
Preprint. Discussion started: 8 November 2021

Atmospheric Chemistry and Physics Discussions

616 Chen, L., Huang, Y., Xue, Y., Jia, Z., and Wang, W.: Atmospheric oxidation of 1-butene initiated
617 by OH radical: Implications for ozone and nitrous acid formations, Atmos. Environ., 244,
618 118010-118021, https://doi.org/10.1016/j.atmosenv.2020.118010, 2021.
619 Chen, L., Huang, Y., Xue, Y., Shen, Z., Cao, J., and Wang, W.: Mechanistic and kinetics
620 investigations of oligomer formation from Criegee intermediate reactions with hydroxyalkyl
621 hydroperoxides, Atmos. Chem. Phys., 19, 4075-4091,
622 https://doi.org/10.5194/acp-19-4075-2019, 2019.
623 Chen, L., Wang, W., Zhou, L., Wang, W., Liu, F., Li, C., and Lü, J.: Role of water clusters in the
624 reaction of the simplest Criegee intermediate CH_2OO with water vapour, Theor. Chem. Acc.,
625 135, 252-263, https://doi.org/10.1007/s00214-016-1998-2, 2016a.
626 Chen, L., Wang, W., Wang, W., Liu, Y., Liu, F., Liu, N., and Wang, B.: Water-catalyzed
627 decomposition of the simplest Criegee intermediate CH_2OO, Theor. Chem. Acc., 135,
628 131-143, https://doi.org/10.1007/s00214-016-1894-9, 2016b.
629 Chhantyal-Pun, R., Welz, O., Savee, J. D., Eskola, A. J., Lee, E. P. F., Blacker, L., Hill, H. R.,
630 Ashcroft, M., Khan, M. A. H., Lloyd-Jones, G. C., Evans, L., Rotavera, B., Huang, H.,
631 Osborn, D. L., Mok, D. K. W., Dyke, J. M., Shallcross, D. E., Percival, C. J., Orr-Ewing, A. J.,
632 and Taatjes, C. A.: Direct measurements of unimolecular and bimolecular reaction kinetics of
633 the Criegee intermediate $(CH_3)_2COO$, J. Phys. Chem. A, 121, 4-15,
634 https://doi.org/10.1021/acs.jpca.6b07810, 2017.
635 Crounse, J. D., Nielsen, L. B., Jørgensen, S., Kjaergaard, H. G., and Wennberg, P. O.:
636 Autoxidation of organic compounds in the atmosphere, J. Phys. Chem. Lett., 4, 3513-3520,
637 https://doi.org/10.1021/jz4019207, 2013.
638 Dillon, T. J., and Crowley, J. N.: Direct detection of OH formation in the reactions of HO_2 with
639 $CH_3C(O)O_2$ and other substituted peroxy radicals, Atmos. Chem. Phys., 8, 4877-4889,
640 https://doi.org/10.5194/acp-8-4877-2008, 2008.
641 Eckart, C.: The penetration of a potential barrier by electrons, Phys. Rev., 35, 1303-1309,
642 https://doi.org/10.1103/PhysRev.35.1303, 1930.
643 Ehn, M., Berndt, T., Wildt, J., and Mentel, T.: Highly oxygenated molecules from atmospheric
644 autoxidation of hydrocarbons: a prominent challenge for chemical kinetics studies, Int. J.
645 Chem. Kinet., 49, 821-831, https://doi.org/10.1002/kin.21130, 2017.
646 Ehn, M., Thornton, J. A., Kleist, E., Sipilä, M., Junninen, H., Pullinen, I., Springer, M., Rubach, F.,
647 Tillmann, R., Lee, B., Lopez-Hilfiker, F., Andres, S., Acir, I. H., Rissanen, M., Jokinen,T.,
648 Schobesberger, S., Kangasluoma, J., Kontkanen, J., Nieminen, T., Kurtén, T., Nielsen, L. B.,
649 Jørgensen, S., Kjaergaard, H. G., Canagaratna, M., Maso, M. D., Berndt, T., Petäjä, T.,
650 Wahner, A., Kerminen, V. M., Kulmala, M., Worsnop, D. R., Wildt, J., and Mentel T. F.: A
651 large source of low-volatility secondary organic aerosol, Nature, 506, 476-9,
652 10.1038/nature13032, 2014.
653 Francisco, J. S., and Eisfeld, W.: Atmospheric oxidation mechanism of hydroxymethyl
654 hydroperoxide, J. Phys. Chem. A, 113, 7593-7600, https://doi.org/10.1021/jp901735z, 2009,
655 Frisch, M. J., Trucks, G. W., Schlegel, H. B., Scuseria, G. E., Robb, M. A., Cheeseman, J. R.,
656 Montgomery, J. A. Jr., Vreven, T., Kudin, K. N., Burant, J. C., Millam, J. M., Iyengar, S. S.,
657 Tomasi, J., Barone, V., Mennucci. B., Cossi, M., Scalmani, G., Rega, N., Petersson, G. A.,
658 Nakatsuji, H., Hada, M., Ehara, M., Toyota, K., Fukuda, R., Hasegawa, J., Ishida, M.,
659 Nakajima, T., Honda, Y., Kitao, O., Nakai, H., Klene, M., Li, X., Knox, J. E., Hratchian, H. P.,

https://doi.org/10.5194/acp-2021-890
Preprint. Discussion started: 8 November 2021

Atmospheric Chemistry and Physics Discussions

660 Cross, J. B., Adamo, C., Jaramillo, J., Gomperts, R., Stratmann, R. E., Yazyev, O., Austin, A.
661 J., Cammi, R., Pomelli, C., Ochterski, J. W., Ayala, P. Y., Morokuma, K., Voth, G. A.,
662 Salvador, P., Dannenberg, J. J., Zakrzewski, V. G., Dapprich, S., Daniels, A. D., Strain, M. C.,
663 Farkas, O., Malick, D. K., Rabuck, A. D., Raghavachari, K., Foresman, J. B., Ortiz, J. V., Cui,
664 Q., Baboul, A. G., Clifford, S., Cioslowski, J., Stefanov, B. B., Liu, G., Liashenko, A.,
665 Piskorz, P., Komaromi, I., Martin, R. L., Fox, D. J., Keith, T., Al-Laham, M. A., Peng, C. Y.,
666 Nanayakkara, A., Challacombe, M., Gill, P. M. W., Johnson, B., Chen, W., Wong, M. W.,
667 Gonzalez, C., and Pople, J. A.: Gaussian 09, Revision D.01; Gaussian, Inc.: Wallingford, CT,
668 2009.
669 Fukui, K.: The path of chemical reactions - the IRC approach, Acc. Chem. Res., 14, 363-368,
670 https://doi.org/10.1021/ar00072a001, 1981.
671 Gilbert, R. G., Smith, S. C.: Theory of unimolecular and recombination reactions; Blackwell
672 Scientific: Carlton, Australia, 1990.
673 Gligorovski, S., Strekowski, R., Barbati, S., and Vione, D.: Environmental implications of
674 hydroxyl radicals (OH), Chem. Rev., 115, 13051-13092, https://doi.org/10.1021/cr500310b,
675 2015.
676 Glowacki, D. R., Liang, C. H., Morley, C., Pilling, M. J., and Robertson, S. H.: MESMER: an
677 open-source master equation solver for multi-energy well reactions, J. Phys. Chem. A, 116,
678 9545-9560, https://doi.org/10.1021/jp3051033, 2012.
679 Gong, Y., and Chen, Z.: Quantification of the role of stabilized Criegee intermediates in the
680 formation of aerosols in limonene ozonolysis, Atmos. Chem. Phys., 21, 813-829,
681 https://doi.org/10.5194/acp-21-813-2021, 2021.
682 Hasan, G., Salo, V. T., Valiev, R. R., Kubečka, J., and Kurtén, T.: Comparing reaction routes for
683 ^{3}(RO…OR') intermediates formed in peroxy radical self- and cross-reactions, J. Phys. Chem.
684 A, 124, 8305-8320, https://doi.org/10.1021/acs.jpca.0c05960, 2020.
685 Hofzumahaus, A., Rohrer, F., Lu, K., Bohn, B., Brauers, T., Chang, C. C., Fuchs, H., Holland, F.,
686 Kita, K., Kondo, Y., Li, X., Lou, S., Shao, M., Zeng, L., Wahner, A., and Zhang, Y.:
687 Amplified trace gas removal in the troposphere, Science, 324, 1702-1704,
688 https://doi.org/10.1126/science.1164566, 2009.
689 Holbrook, K. A., Pilling, M. J., Robertson, S. H., Robinson, P. J.: Unimolecular reactions, 2nd ed.;
690 Wiley: New York, 1996.
691 Huang, H. L., Chao, W., and Lin, J. J. M.: Kinetics of a Criegee intermediate that would survive
692 high humidity and may oxidize atmospheric SO_2, Proc. Natl. Acad. Sci. U.S.A., 112,
693 10857-10862, https://doi.org/10.1073/pnas.1513149112, 2015.
694 Iyer, S., Reiman, H., Møller, K. H., Rissanen, M. P., Kjaergaard, H. G., and Kurtén, T.:
695 Computational investigation of RO_2 + HO_2 and RO_2 + RO_2 reactions of monoterpene derived
696 first-generation peroxy radicals leading to radical recycling, J. Phys. Chem. A, 122,
697 9542-9552, https://doi.org/10.1021/acs.jpca.8b09241, 2018.
698 Iyer, S., Rissanen, M. P., Valiev, R., Barua, S., Krechmer, J. E., Thornton, J., Ehn, M., Kurtén, T.:
699 Molecular mechanism for rapid autoxidation in α-pinene ozonolysis, Nat. Commun.,
700 https://doi.org/10.1038/s41467-021-21172-w, 12, 878-883, 2021.
701 Jokinen, T., Sipilä, M., Richters, S., Kerminen, V. M., Paasonen, P., Stratmann, F., Worsnop, D.,
702 Kulmala, M., Ehn, M., Herrmann, H., and Berndt, T.: Rapid autoxidation forms highly
703 oxidized RO_2 radicals in the atmosphere, Angew. Chem. Int. Ed., 53, 14596-14600,

https://doi.org/10.5194/acp-2021-890
Preprint. Discussion started: 8 November 2021

http://dx.doi.org/10.1002/anie.201408566, 2014.

Khan, M. A. H., Percival, C. J., Caravan, R. L., Taatjes, C. A., and Shallcross, D. E.: Criegee intermediates and their impacts on the troposphere, Environ. Sci.: Processes Impacts, 20, 437-453, https://doi.org/10.1039/C7EM00585G, 2018.

Kumar, M., and Francisco, J. S.: Red-light-induced decomposition of an organic peroxy radical: a new source of the HO_2 radical, Angew. Chem. Int. Ed., 54, 15711-15714, https://doi.org/10.1002/anie.201509311, 2015.

Kumar, M., Busch, D. H., Subramaniam, Bala., and Thompson, W. H.: Role of tunable acid catalysis in decomposition of α-hydroxyalkyl hydroperoxides and mechanistic implications for tropospheric chemistry, J. Phys. Chem. A, 118, 9701-9711, https://doi.org/10.1021/jp505100x, 2014.

Lee, R., Gryn'ova, G., Ingold, K. U., and Coote, M. L.: Why are sec-alkylperoxyl bimolecular self-reactions orders of magnitude faster than the analogous reactions of tert-alkylperoxyls? The unanticipated role of CH hydrogen bond donation, Phys. Chem. Chem. Phys., 18, 23673-23679, http://dx.doi.org/10.1039/C6CP04670C, 2016.

Lester, M. I., and Klippenstein, S. J.: Unimolecular decay of Criegee intermediates to OH radical products: prompt and thermal decay processes, Acc. Chem. Res., 51, 978-985, https://doi.org/10.1021/acs.accounts.8b00077, 2018.

Liu, L., Bei, N., Wu, J., Liu, S., Zhou, J., Li, X., Yang, Q., Feng, T., Cao, J., Tie, X., and Li, G.: Effects of stabilized Criegee intermediates (sCIs) on sulfate formation: a sensitivity analysis during summertime in Beijing-Tianjin-Hebei (BTH), China. Atmos. Chem. Phys., 19, 13341-13354, https://doi.org/10.5194/acp-19-13341-2019, 2019.

Lu, T.: Molclus program, Version 1.9.3, http://www.keinsci.com/research/molclus.html (accessed Feb. 10, 2020).

Ma, F., Guo, X., Xia, D., Xie, H. B., Wang, Y., Elm, J., Chen, J., and Niu, J., Atmospheric chemistry of allylic radicals from isoprene: a successive cyclization-driven autoxidation mechanism, Environ. Sci. Technol., 55, 4399-4409, https://doi.org/10.1021/acs.est.0c07925, 2021.

Møller, K. H., Berndt, T., and Kjaergaard, H. G.: Atmospheric autoxidation of amines, Environ. Sci. Technol., 54, 11087-11099, https://doi.org/10.1021/acs.est.0c03937, 2020.

Møller, K. H., Otkjær, R. V., Hyttinen, N., Kurtén, T., and Kjaergaard, H. G.: Cost-effective implementation of multiconformer transition state theory for peroxy radical hydrogen shift reactions, J. Phys. Chem. A, 120, 10072-10087, https://doi.org/10.1021/acs.jpca.6b09370, 2016.

Nozière, B., and Vereecken, L.: Direct observation of aliphatic peroxy radical autoxidation and water effects: an experimental and theoretical study, Angew. Chem. Int. Ed., 58, 13976-13982, http://dx.doi.org/10.1002/anie.201907981, 2019.

Orlando, J. J., and Tyndall, G. S.: Laboratory studies of organic peroxy radical chemistry: an overview with emphasis on recent issues of atmospheric significance, Chem. Soc. Rev., 41, 6294-6317, https://doi.org/10.1039/c2cs35166h, 2012.

Perring, A. E., Pusede, S. E., and Cohen, R. C.: An observational perspective on the atmospheric impacts of alkyl and multifunctional nitrates on ozone and secondary organic aerosol, Chem. Rev., 113, 5848-5870, https://doi.org/10.1021/cr300520x, 2013,

Qiu, J. T., Ishizuka, S., Tonokura, K., Colussi, A. J., and Enami, S.: Water dramatically accelerates

https://doi.org/10.5194/acp-2021-890
Preprint. Discussion started: 8 November 2021

Atmospheric Chemistry and Physics Discussions

748 the decomposition of α-hydroxyalkyl-hydroperoxides in aerosol particles, J. Phys. Chem.
749 Lett., 10, 5748-5755, https://doi.org/10.1021/acs.jpclett.9b01953, 2019.
750 Rissanen, M. P., Kurtén, T., Sipilä, M., Thornton, J. A., Kangasluoma, J., Sarnela, N., Junninen, H.,
751 Jørgensen, S., Schallhart, S., Kajos, M. K., Taipale, R., Springer, M., Mentel, T. F.,
752 Ruuskanen, T., Petäjä, T., Worsnop, D. R., Kjaergaard, H. G., and Ehn, M.: The formation of
753 highly oxidized multifunctional products in the ozonolysis of cyclohexene, J. Am. Chem.
754 Soc., 136, 15596-15606, https://doi.org/10.1021/ja507146s, 2014.
755 Russell, G. A.: Deuterium-isotope effects in the autoxidation of aralkyl hydrocarbons. Mechanism
756 of the interaction of peroxy radicals, J. Am. Chem. Soc., 79, 3871-3877,
757 https://doi.org/10.1021/ja01571a068, 1957.
758 Ryzhkov, A. B., and Ariya, P. A.: A theoretical study of the reactions of carbonyl oxide with water
759 in atmosphere: the role of water dimer, Chem. Phys. Lett., 367, 423-429,
760 https://doi.org/10.1016/S0009-2614(02)01685-8, 2003.
761 Smith, M. C., Chang, C. H., Chao, W., Lin, L. C., Takahashi, K., Boering, K. A., and Lin, J. J. M.:
762 Strong negative temperature dependence of the simplest Criegee intermediate CH_2OO
763 reaction with water dimer, J. Phys. Chem. Lett., 6, 2708-2713,
764 https://doi.org/10.1021/acs.jpclett.5b01109, 2015.
765 Stone, D., Whalley, L. K., and Heard, D. E.: Tropospheric OH and HO_2 radicals: field
766 measurements and model comparisons, Chem. Soc. Rev., 41, 6348-6404,
767 https://doi.org/10.1039/c2cs35140d, 2012.
768 Taatjes, C. A., Welz, O., Eskola, A. J., Savee, J. D., Scheer, A. M., Shallcross, D. E., Rotavera, B.,
769 Lee, E. P. F., Dyke, J. M., Mok, D. K. W., Osborn, D. L., and Percival, C. J.: Direct
770 measurements of conformer-dependent reactivity of the Criegee intermediate CH_3CHOO,
771 Science, 340, 177-180, https://doi.org/10.1126/science.1234689, 2013.
772 Taatjes, C. A.: Criegee intermediates: what direct production and detection can teach us about
773 reactions of carbonyl oxides, Annu. Rev. Phys. Chem., 68, 183-207,
774 https://doi.org/10.1146/annurev-physchem-052516-050739, 2017.
775 Valiev, R. R., Hasan, G., Salo, V. T., Kubečka, J., and Kurten, T.: Intersystem crossings drive
776 atmospheric gas-phase dimer formation, J. Phys. Chem. A, 123, 6596-6604,
777 https://doi.org/10.1021/acs.jpca.9b02559, 2019.
778 Vereecken, L., and Nozière, B.: H migration in peroxy radicals under atmospheric conditions,
779 Atmos. Chem. Phys., 20, 7429-7458, https://doi.org/10.5194/acp-20-7429-2020, 2020.
780 Wang, S., Riva, M., Yan, C., Ehn, M., and Wang, L.: Primary formation of highly oxidized
781 multifunctional products in the OH-initiated oxidation of isoprene: a combined theoretical
782 and experimental study, Environ. Sci. Technol., 52, 12255-12264,
783 https://doi.org/10.1021/acs.est.8b02783, 2018.
784 Wang, S., Wu, R., Berndt, T., Ehn, M., and Wang, L.: Formation of highly oxidized radicals and
785 multifunctional products from the atmospheric oxidation of alkylbenzenes, Environ. Sci.
786 Technol., 51, 8442-8449, https://doi.org/10.1021/acs.est.7b02374, 2017.
787 Winiberg, F. A. F., Dillon, T. J., Orr, S. C., Groß, C. B. M., Bejan, I., Brumby, C. A., Evans, M. J.,
788 Smith, S. C., Heard, D. E., and Seakins, P. W.: Direct measurements of OH and other product
789 yields from the $HO_2 + CH_3C(O)O_2$ reaction, Atmos. Chem. Phys., 16, 4023-4042,
790 https://doi.org/10.5194/acp-16-4023-2016, 2016.
791 Xu, L., Kollman, M. S., Song, C., Shilling, J. E., and Ng, N. L.: Effects of NO_x on the volatility of

https://doi.org/10.5194/acp-2021-890
Preprint. Discussion started: 8 November 2021

Atmospheric Chemistry and Physics Discussions

792 secondary organic aerosol from isoprene photooxidation, Environ. Sci. Technol., 48,
793 2253-2262, https://doi.org/10.1021/es404842g, 2014.
794 Xu, L., Møller, K. H., Crounse, J. D., Kjaergaard, H. G., and Wennberg, P. O.: New insights into
795 the radical chemistry and product distribution in the OH-initiated oxidation of benzene,
796 Environ. Sci. Technol., 54, 13467-13477, https://doi.org/10.1021/acs.est.0c04780, 2020.
797 Zhang, P., Wang, W., Zhang, T., Chen, L., Du, Y., Li, C., and Lv, J.: Theoretical study on the
798 mechanism and kinetics for the self-reaction of $C_2H_5O_2$ radicals, J. Phys. Chem. A, 116,
799 4610-4620, http://dx.doi.org/10.1021/jp301308u, 2012.
800 Zhao, Y., and Truhlar, D. G.: The M06 suite of density functionals for main group
801 thermochemistry, thermochemical kinetics, noncovalent interactions, excited states, and
802 transition elements: two new functionals and systematic testing of four M06-class functionals
803 and 12 other functionals, Theor. Chem. Acc., 120, 215-241,
804 http://dx.doi.org/10.1007/s00214-007-0310-x, 2008.
805 Zhao, Y., and Truhlar, D. G.: A new local density functional for main-group thermochemistry,
806 transition metal bonding, thermochemical kinetics, and noncovalent interactions, J. Chem.
807 Phys., 125, 194101-194119, http://dx.doi.org/10.1063/1.2370993, 2006.
808 Zheng, J., and Truhlar, D. G.: Direct dynamics study of hydrogen-transfer isomerization of
809 1-pentyl and 1-hexyl radicals, J. Phys. Chem. A, 113, 11919-11925,
810 http://dx.doi.org/10.1021/jp903345x, 2009.
811 Zheng, J., Xu, X., and Truhlar, D. G.: Minimally augmented Karlsruhe basis sets, Theor. Chem.
812 Acc., 128, 295-305, https://doi.org/10.1007/s00214-010-0846-z, 2011.
813 Zhong, J., Kumar, M., Francisco, J. S., and Zeng, X. C.: Insight into chemistry on cloud/aerosol
814 water surfaces, Acc. Chem. Res., 51, 1229-1237,
815 https://doi.org/10.1021/acs.accounts.8b00051, 2018.
816 Zhou, X., Liu, Y., Dong, W., and Yang, X.: Unimolecular reaction rate measurement of
817 syn-CH_3CHOO, J. Phys. Chem. Lett., 10, 4817-4821,
818 https://doi.org/10.1021/acs.jpclett.9b01740, 2019.
819 Zhu, C., Kumar, M., Zhong, J., Li, L., Francisco, J. S., and Zeng, X. C.: New mechanistic
820 pathways for Criegee-water chemistry at the air/water interface, J. Am. Chem. Soc., 138,
821 11164-11169, https://doi.org/10.1021/jacs.6b04338, 2016.
822

https://doi.org/10.5194/acp-2021-890
Preprint. Discussion started: 8 November 2021

Atmospheric Chemistry and Physics Discussions

Table 1 Relative free energies (kcal mol^{-1}) for the stationary points, free energy ($\Delta G_a^{\#}$) barriers and reaction free energies (ΔG) for the elementary pathways of OH radical reactions with distinct HHPs calculated at the M06-2X/ma-TZVP//M06-2X/6-311+G(2df,2p) level of theory. Labels A, B, C, and D are defined in Figure 2

Entry	R1	R2	A	B	C	D	$\Delta G_a^{\#}$	ΔG
$HO\text{-}CH_2OOH$ + OH								
R1(O_1-H_1)	H	H	2.5	8.9	-8.5	-13.7	6.4	-13.7
R2(C_1-H1)	H	H	4.2	9.3	-20.4	-21.7	5.1	-21.7
R3(C_1-H2)	H	H	3.1	8.9	-20.6	-21.9	5.8	-21.9
R4(O_3-H_2)	H	H	4.2	5.7	-29.0	-30.2	1.5	-30.2
$HO\text{-}CH(CH_3)OOH$ + OH								
R1'(O_1-H_1)	CH_3	H	1.7	8.9	-11.6	-12.8	7.2	-12.8
R2'(C_1-H)	CH_3	H	5.5	7.7	-17.5	-20.9	2.2	-20.9
R3'(-CH_3(R1))	CH_3	H	4.0	9.9	-14.4	-15.1	5.9	-15.1
R4'(O_3-H_2)	CH_3	H	3.9	5.6	-29.2	-30.5	1.7	-30.5
$HO\text{-}C(CH_3)_2OOH$ + OH								
R1"(O_1-H_1)	CH_3	CH_3	1.8	9.2	0.9	-3.4	7.4	-3.4
R2"(-CH_3(R1))	CH_3	CH_3	2.0	10.0	-14.4	-15.4	8.0	-15.4
R3"(-CH_3(R2))	CH_3	CH_3	4.8	10.6	-13.8	-15.0	5.8	-15.0
R4"(O_3-H_2)	CH_3	CH_3	1.8	7.3	29.8	-31.4	5.5	-31.4

https://doi.org/10.5194/acp-2021-890
Preprint. Discussion started: 8 November 2021

Atmospheric Chemistry and Physics Discussions

Figure Captions:

Figure 1. The structures of distinct HHPs formed from the reactions of water with CH_2OO, *anti*-CH_3CHOO and $(CH_3)_2COO$

Figure 2. Schematic profile for the initial reactions of OH radical with distinct HHPs

Figure 3. PES ($\Delta G_a^{\#}$ and $\Delta E_a^{\#}$, in italics) for the self-reaction of $HOCH_2OO$ radicals predicted at the M06-2X/ma-TZVP//M06-2X/6-311+G(2df,2p) level of theory

Figure 4. PES ($\Delta G_a^{\#}$ and $\Delta E_a^{\#}$, in italics) for the self-reaction of $HOCH_3CHOO$ radicals predicted at the M06-2X/ma-TZVP//M06-2X/6-311+G(2df,2p) level of theory

Figure 5. PES ($\Delta G_a^{\#}$ and $\Delta E_a^{\#}$, in italics) for the self-reaction of $HO(CH_3)_2COO$ radicals predicted at the M06-2X/ma-TZVP//M06-2X/6-311+G(2df,2p) level of theory

Figure 6. PES ($\Delta G_a^{\#}$ and $\Delta E_a^{\#}$, in italics) for the reactions of HO_2 radical with distinct RO_2 radicals predicted at the M06-2X/ma-TZVP//M06-2X/6-311+G(2df,2p) level of theory

Figure 7. PES ($\Delta G_a^{\#}$ and $\Delta E_a^{\#}$, in italics) for the autoxidation of $HOCH_2OO$ radical predicted at the M06-2X/ma-TZVP//M06-2X/6-311+G(2df,2p) level of theory

Figure 8. PES ($\Delta G_a^{\#}$ and $\Delta E_a^{\#}$, in italics) for the reaction of $HOCH_2OO$ radical with NO predicted at the M06-2X/ma-TZVP//M06-2X/6-311+G(2df,2p) level of theory (the superscript a is calculated at the MP2/ma-TZVP//MP2/6-311+G(2df,2p) level)

Figure 9. PES ($\Delta G_a^{\#}$ and $\Delta E_a^{\#}$, in italics) for the reaction of $HOCH_3CHOO$ radical with NO predicted at the M06-2X/ma-TZVP//M06-2X/6-311+G(2df,2p) level of theory (the superscript a is calculated at the MP2/ma-TZVP//MP2/6-311+G(2df,2p) level)

Figure 10. PES ($\Delta G_a^{\#}$ and $\Delta E_a^{\#}$, in italics) for the reaction of $HO(CH_3)_2COO$ radical with NO predicted at the M06-2X/ma-TZVP//M06-2X/6-311+G(2df,2p) level of theory (the superscript a is calculated at the MP2/ma-TZVP//MP2/6-311+G(2df,2p) level)

https://doi.org/10.5194/acp-2021-890
Preprint. Discussion started: 8 November 2021

Atmospheric Chemistry and Physics Discussions

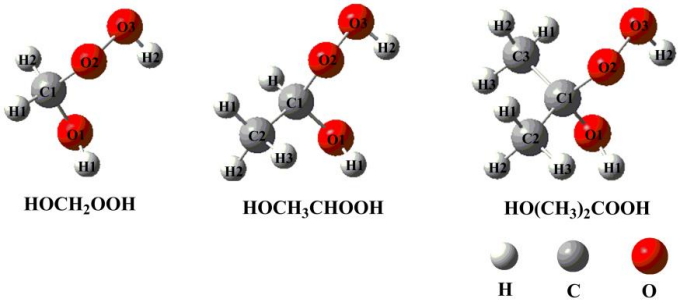

Figure 1.

https://doi.org/10.5194/acp-2021-890
Preprint. Discussion started: 8 November 2021

Atmospheric Chemistry and Physics Discussions

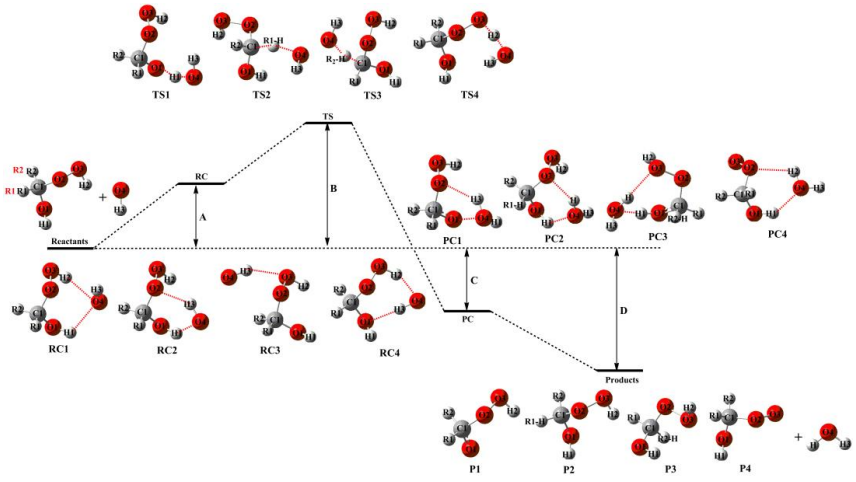

Figure 2.

https://doi.org/10.5194/acp-2021-890
Preprint. Discussion started: 8 November 2021

Atmospheric Chemistry and Physics Discussions

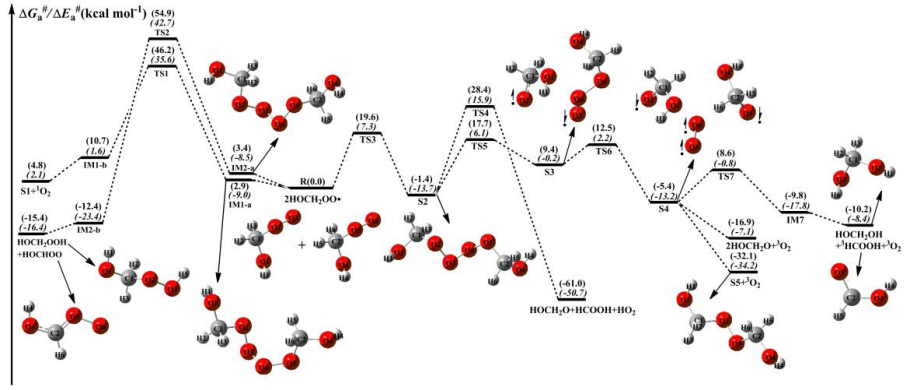

Figure 3.

https://doi.org/10.5194/acp-2021-890
Preprint. Discussion started: 8 November 2021

Atmospheric Chemistry and Physics Discussions

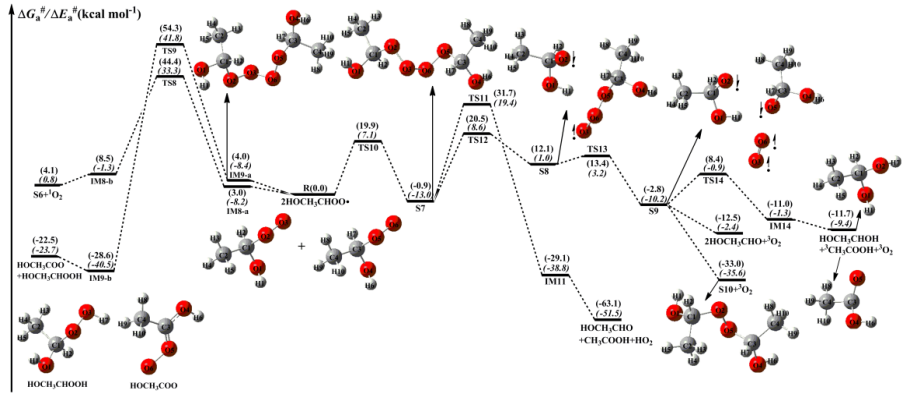

Figure 4.

https://doi.org/10.5194/acp-2021-890
Preprint. Discussion started: 8 November 2021

Atmospheric Chemistry and Physics Discussions

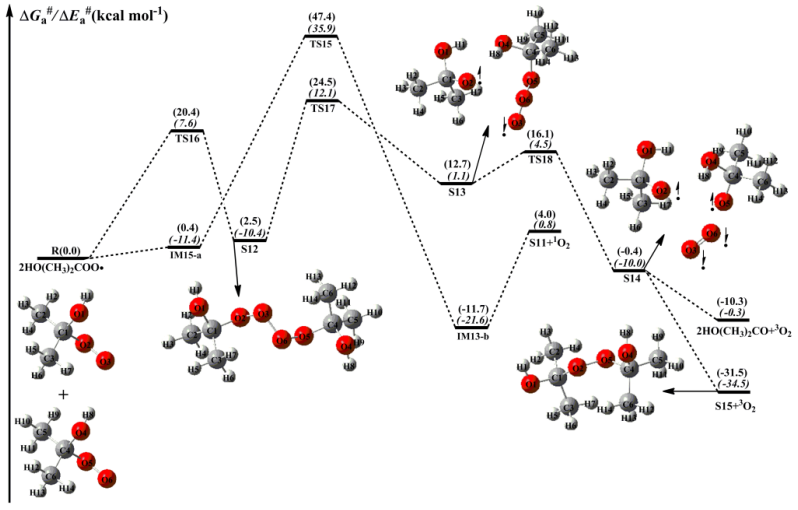

Figure 5.

https://doi.org/10.5194/acp-2021-890
Preprint. Discussion started: 8 November 2021

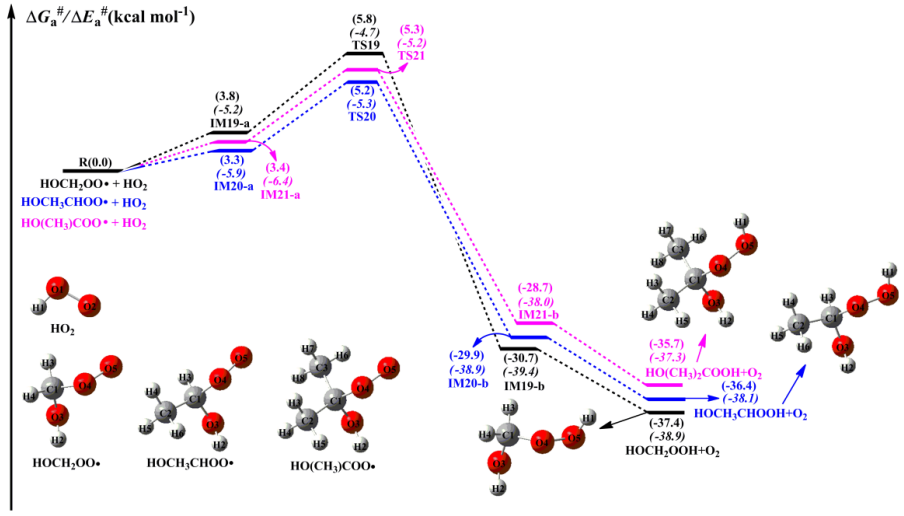

Figure 6.

https://doi.org/10.5194/acp-2021-890
Preprint. Discussion started: 8 November 2021

Atmospheric Chemistry and Physics Discussions

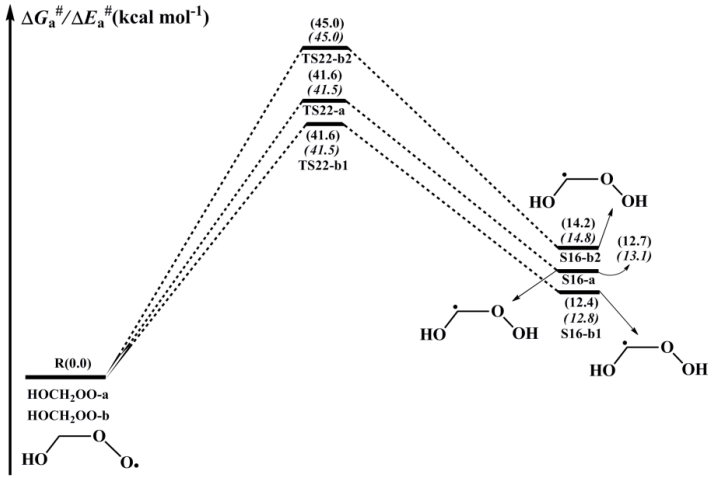

863

864 **Figure 7.**

https://doi.org/10.5194/acp-2021-890
Preprint. Discussion started: 8 November 2021

Atmospheric Chemistry and Physics Discussions

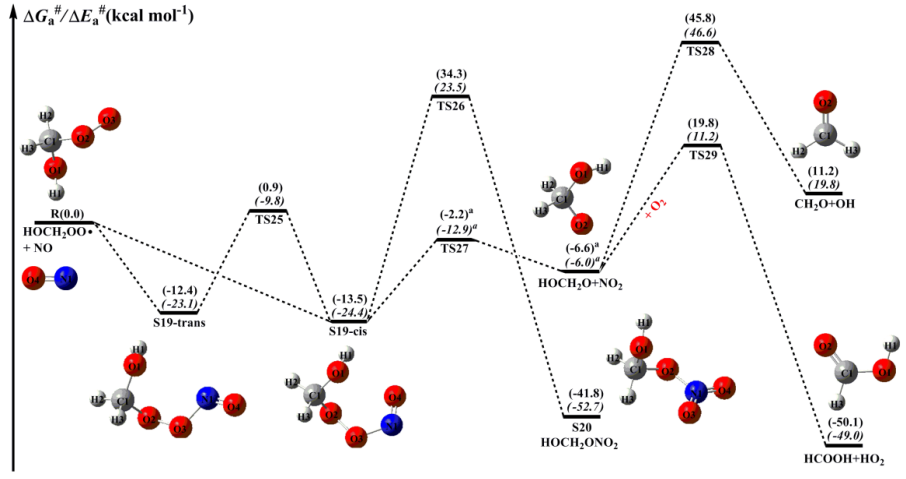

865

866 **Figure 8.**

https://doi.org/10.5194/acp-2021-890
Preprint. Discussion started: 8 November 2021

Atmospheric Chemistry and Physics Discussions

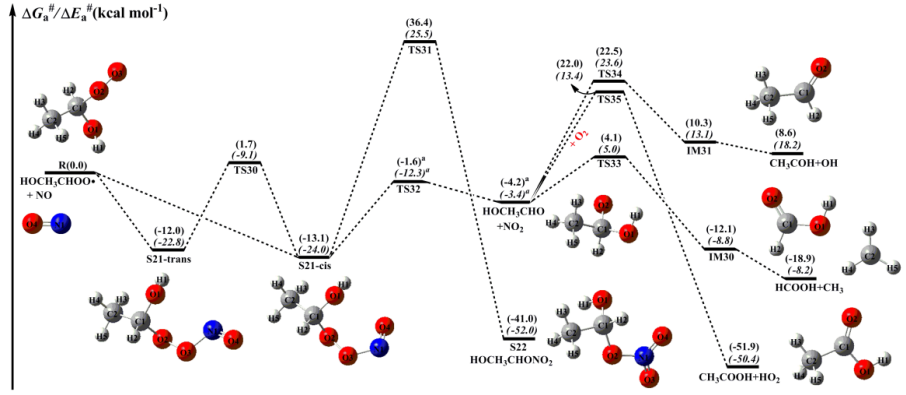

867
868 **Figure 9.**

https://doi.org/10.5194/acp-2021-890
Preprint. Discussion started: 8 November 2021

Atmospheric Chemistry and Physics Discussions

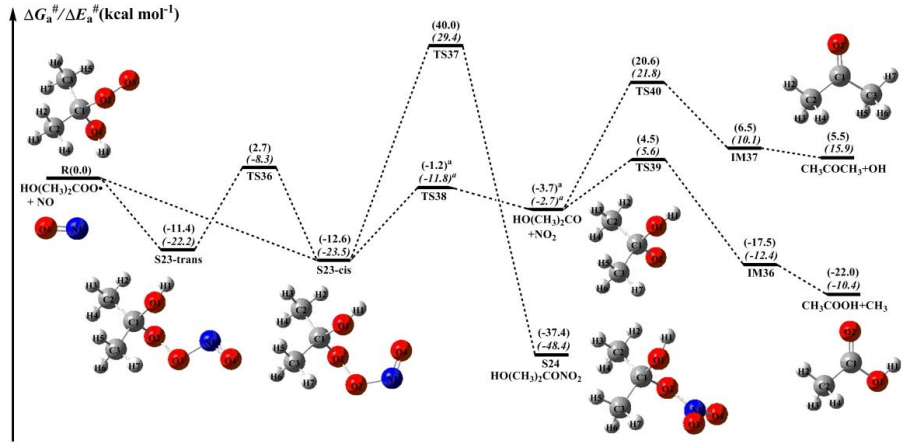

Figure 10.